PHYSOR 2012 Advances in Reactor Physics Linking Research, Industry, and Education
Knoxville, Tennessee, USA, April 15-20, 2012, on CD-ROM, American Nuclear Society, LaGrange Park, IL (2012)

EXPERIMENTAL AND COMPUTATIONAL STUDY OF THE FLUX SPECTRUM IN MATERIALS IRRADIATION FACILITIES OF THE HIGH FLUX ISOTOPE REACTOR

Thomas Daly
Department of Nuclear Engineering
University of Tennessee
315 Pasqua Engineering Building
Knoxville, TN 37996-2300
tdaly1@utk.edu

Joel McDuffee
Oak Ridge National Laboratory
P.O. Box 2008
Oak Ridge, TN 37831
mcduffeej@ornl.gov

ABSTRACT

This report compares the available experimental neutron flux data in the High Flux Isotope Reactor (HFIR) to computational models of the HFIR loosely based on the experimental loading of Cycle 400. Over the last several decades, many materials irradiation experiments have included fluence monitors that were subsequently used to reconstruct a coarse-group energy-dependent flux spectrum. Experimental values for thermal and fast neutron flux in the flux trap about the midplane are found to be 1.73 ± 0.20 and $1.06 \pm 0.04 \cdot 10^{15} \frac{\mathrm{n}}{\mathrm{cm}^2-\mathrm{sec}}$, respectively. The reactor physics code MCNP is used to calculate neutron flux in the HFIR at irradiation locations. The computational results are shown to correspond closely to experimental data for thermal and fast neutron flux with calculated percent differences ranging from 0.55–13.20%.

Key Words: irradiation experiments, HFIR, MCNP

1. INTRODUCTION

The High Flux Isotope Reactor (HFIR) is an 85 MW research reactor located at Oak Ridge National Laboratory (ORNL) in Oak Ridge, Tennessee. The reactor has one of the highest steady-state neutron fluxes in the world and as such is ideally suited for isotope production and neutron interrogation experiments. Currently the HFIR is used for isotope production, materials irradiation, and as a source for neutron scattering experiments.

In order to design and analyze irradiation experiments, it is necessary to have a reliable understanding of the spatially varying neutron flux spectrum. Over the last several decades, many materials irradiation experiments have included fluence monitors that were subsequently used to reconstruct a coarse-group energy-dependent flux spectrum. This report compares the available experimental data to computational models of HFIR loosely based on the experimental loading of Cycle 400. Each of the primary irradiation target facilities in HFIR is analyzed at the beginning and end of cycle: metrics include four-group axial flux distribution and a 69-group flux spectrum.

1.1. Materials Irradiation Facilities at the HFIR

Materials to be irradiated are typically housed in cylindrical aluminum or stainless steel capsules and placed in one of the experimental target locations in the reactor at varying axial locations. The irradiation positions most often used can be broadly categorized into three groups: the flux-trap target (FT) locations, the Removable Beryllium (RB) reflector region, and the Vertical Experiment Facilities (VXF) located in the permanent reflector. The irradiation facilities and four horizontal beam tubes are shown in Fig. 1. The FT target locations are located in the center of the core, the RB facilities are located in the purple ring, and the VXF targets are located in the permanent reflector shown in green.

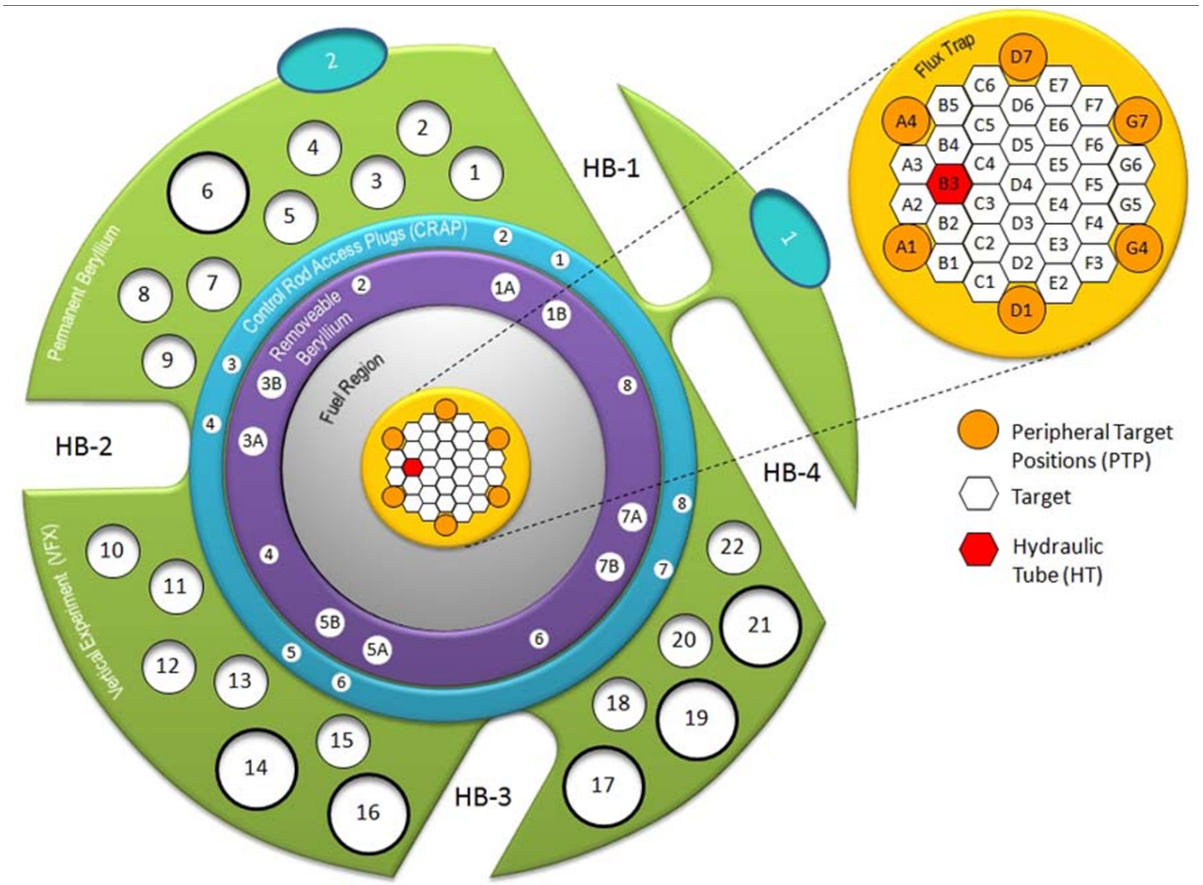

Figure 1. Plan view of the HFIR target positions [1].

1.1.1. Flux trap region

The FT region has the highest thermal fluxes in the reactor, reaching $2.5 \cdot 10^{15} \frac{\mathrm{n}}{\mathrm{cm}^2-\mathrm{sec}}$, as well as the highest heat generation rates (approximately $43 \cdot \mathrm{W/g}$ in aluminum). As shown in Fig. 1, this region contains a total of 37 target locations, including one Hydraulic Tube (HT) and six

Peripheral Target Position (PTP) facilities. Using the HT allows materials to be irradiated from a few minutes up to one full cycle. The targets closest to the fuel, the PTP locations, have the highest heat generation and fast neutron flux of all irradiation locations in the reactor.

2. EXPERIMENTAL NEUTORN FLUX MEASUREMENTS

A large amount of experimental data has been produced and published over the lifetime of the reactor, although the data have never been compiled. The data in this paper consist of more than 71 experiments spanning 20 years [4] [5] [6] [7] [8] [9] [10] [11] [12] [13] [14] [15] [16] [17] [18] [19] [21] [22]. Fluence values from the experiments are most often obtained from activation and helium accumulation monitors. Experimental data shown below are split into three groups: the PTP, the remaining FT experiments, and those in the RB positions. Most experiments were performed in the outermost ring of the FT and in the PTP, corresponding to the 5th and 6th Monte Carlo N-Particle (MCNP) groups described in Section 3.

Most experiments reported three energy groups — thermal, intermediate, and fast. The energy bounds of the experimental flux groups are not reported consistently. All contain a thermal flux group defined as $E < 0.5\ \mathrm{eV}$ and an intermediate energy group defined as everything between thermal and fast. The fast group is given as either $E > 0.1\ \mathrm{MeV}$ or $E > 0.11\ \mathrm{MeV}$. Most commonly, the fast flux lower bound is given as $0.1\ \mathrm{MeV}$. All fast flux results from groups defined as either $E > 0.1$ or $E > 0.11\ \mathrm{MeV}$ are compared together. Those experiments that define fast flux as $E > 0.11\ \mathrm{MeV}$ are noted in their corresponding tables. The data presented contain total, thermal, intermediate, and fast fluxes at the midplane of the reactor. A normalized axial thermal flux distribution given as

$$\phi(z)/\phi_{midplane} = 1 + bz + cz^2 \tag{1}$$

is also included. In Eq. 1, z is the displacement in centimeters from the horizontal midplane of the core whose axis points towards the top of the reactor. Fractional uncertainty of the flux values is calculated as the sample standard deviation divided by the sample mean.

2.1. Experimental Results in Flux Trap Region

Table I contains neutron flux values from 18 experiments located in the PTP region. Each experiment was irradiated in the HFIR at 100 MW for varying amounts of time. The axial fit parameters are all in agreement except for those given in experiments CTR53 and 54, which report a c fit parameter an order of magnitude lower than the others. These values are most likely attributable to a typo in the report [9] and are not included in the calculation of the mean or standard deviation. The experiments were all irradiated in the PTP facilities; however, the exact target locations were not reported. Fractional uncertainties (σ/μ) range from 2.96 to 4.51% for fast and thermal fluxes. Reported values for thermal and fast flux are scaled from 100 to 85 MW, yielding an average of 1.75 and $1.14 \cdot 10^{15} \frac{\mathrm{n}}{\mathrm{cm}^2-\mathrm{sec}}$ at 85 MW, respectively.

Additional experimental FT data are shown in Tables II and III. Experiments that were irradiated at 85 MW are shown in Table II, while the experiments performed at 100 MW are shown in

Table III. The target locations presented in Tables II and III are all in the FT, and most are from the fifth radial group (4.47 cm from center). Fractional uncertainties for the 85 MW FT data range

Table I. Experimental Flux Data – PTP Region

Experiment	**Fit parameter**		**Flux** ($10^{15}\frac{\mathrm{n}}{\mathrm{cm^2-sec}}$)		
	b	**c**	**<0.5 eV**	**0.5 eV–0.1 MeV**	**>0.1 MeV**
CTR30 [7]	5.02E-04	-1.00E-03	2.11	1.70	1.40
CTR31 [4]	1.95E-04	-9.75E-04	2.03	1.62	1.30
CTR32 [4]	1.95E-04	-9.75E-04	2.11	1.64	1.34
CTR34 [4]	1.95E-04	-9.75E-04	1.98	1.59	1.30
CTR35 [4]	1.95E-04	-9.75E-04	1.94	1.56	1.28
CTR36 [7]	5.02E-04	-1.00E-03	1.98	1.61	1.31
CTR39 [5]	1.95E-04	-9.75E-04	2.20	1.70	1.37
CTR40 [6]	1.95E-04	-9.75E-04	2.15	1.66	1.34
CTR41 [6]	1.95E-04	-9.75E-04	2.15	1.66	1.34
CTR42 [6]	1.95E-04	-9.75E-04	2.11	1.63	1.32
CTR43 [6]	1.95E-04	-9.75E-04	2.11	1.63	1.32
CTR44 [6]	1.95E-04	-9.75E-04	2.15	1.65	1.34
CTR45 [6]	1.95E-04	-9.75E-04	2.15	1.65	1.34
CTR46 [7]	5.02E-04	-1.00E-03	1.95	1.58	1.31
CTR47 [8]	5.02E-04	-1.00E-03	1.99	1.69	1.41
CTR48 [8]	5.02E-04	-1.00E-03	1.99	1.69	1.41
CTR53 [9]		-1.02E-04	1.93	1.54	1.31
CTR54 [9]		-1.02E-04	1.93	1.54	1.31
Mean (100 MW)	**2.91E-04**	**-9.83E-04**	**2.05**	**1.63**	**1.34**
Mean (Scaled to 85 MW)			**1.75**	**1.38**	**1.14**
Fractional Uncertainty			**4.51%**	**3.22%**	**2.96%**

from 4.0% for fast to 11.8% for thermal neutrons. The average fast and thermal neutron flux values for this group are calculated to be 1.06 and 1.73 $\cdot 10^{15}\frac{\mathrm{n}}{\mathrm{cm^2-sec}}$, respectively. The JP experiments reported in Table II were carried out at a radial distance of 4.47 cm from the center of the core, while experiments NM192-198 were irradiated in the hydraulic tube (r = 2.93 cm).

2.2. Experimental Results in Removable Beryllium Region

Table IV shows the coarse-group flux values, scaled 85 MW mean flux values, and location information (if available) for five experiments in the RB region. These unshielded experiments are calculated to have percent uncertainties ranging from 11.0–13.9%. The mean fast flux scaled to 85 MW is found to be 0.44 $\cdot 10^{15}\frac{\mathrm{n}}{\mathrm{cm^2-sec}}$.

Table II. Experimental Flux Data (FT 85 MW)

Experiment	Fit parameter		Flux ($10^{15}\frac{\mathrm{n}}{\mathrm{cm}^2-\mathrm{sec}}$)		
	b	c	<0.5 eV	0.5 eV–0.1 MeV	>0.1 MeV
JP-9 [18]	0.00E+00	-9.35E-04	1.65	1.27	1.07
JP-10 [15]	0.00E+00	-9.85E-04	1.51	1.28	1.03
JP-11 [15]	0.00E+00	-9.85E-04	1.51	1.28	1.03
JP-12 [18]	0.00E+00	-9.35E-04	1.65	1.27	1.07
JP-13 [15]	0.00E+00	-9.85E-04	1.51	1.28	1.03
JP-15 [18]	0.00E+00	-9.35E-04	1.65	1.27	1.07
JP-16 [15]	0.00E+00	-9.85E-04	1.51	1.28	1.03
JP-18 [16]	0.00E+00	-9.31E-04	1.77	1.27	1.03
JP-19 [16]	0.00E+00	-9.31E-04	1.77	1.27	1.03
JP-20 [19]	0.00E+00	-9.35E-04	1.93	1.39	1.10
JP-23 [17]	0.00E+00	-1.14E-03	2.02	1.43	1.18
CTR-62 [10]	0.00E+00	-1.06E-03	2.02	1.33	1.08
CTR-63 [10]	0.00E+00	-1.06E-03	2.02	1.33	1.08
Mean	**0.00E+00**	**-9.85E-04**	**1.73**	**1.30**	**1.06**
Fractional Uncertainty			**11.80%**	**4.01%**	**4.03%**
NM192-198 [20]	3.00E-04	-1.10E-03	1.78	1.32	1.05

Table III. Experimental Flux Data (FT 100 MW)

Experiment	Fit parameter		Flux ($10^{15}\frac{\mathrm{n}}{\mathrm{cm}^2-\mathrm{sec}}$)		
	b	c	<0.5 eV	0.5 eV–0.1 MeV	>0.1 MeV
T2 [4]	1.95E-04	-9.75E-04	2.71	1.62	1.26
JP-1 [11]	5.02E-04	-1.00E-03	2.24	1.62	1.32
JP-2 [13]	3.61E-04	-1.01E-03	2.03	1.60	1.33
JP-3 [12]	5.02E-04	-1.00E-03	2.24	1.62	1.32
JP-4 [14]	7.42E-04	-9.80E-04	2.00	1.56	1.33
JP-5 [14]	7.42E-04	-9.80E-04	1.99	1.55	1.32
JP-6 [13]	3.61E-04	-1.01E-03	2.03	1.59	1.32
JP-7 [13]	3.61E-04	-1.01E-03	2.03	1.59	1.32
JP-8 [14]	7.42E-04	-9.80E-04	1.99	1.55	1.32
Mean (100 MW)	5.01E-04	-9.93E-04	2.14	1.59	1.31
Scaled Mean (85 MW)			**1.82**	**1.35**	**1.12**
Fractional Uncertainty			**11.05%**	**1.77%**	**1.48%**

Table IV. Experimental Flux Data (RB)

Experiment	Power level	Fit parameter		Flux ($10^{15}\frac{\mathrm{n}}{\mathrm{cm}^2-\mathrm{sec}}$)		
	(MW)	b	c	<0.5 eV	0.5 eV–0.1 MeV	>0.1 MeV
HFIR-RB1 [22]	100	-2.48E-03	-9.76E-04	1.06	0.77	0.45
HFIR-RB2 [22]	100	-2.48E-03	-9.76E-04	0.98	0.75	0.45
RB1 [23]	10.8	-1.63E-03	-1.28E-03	0.10	0.09	0.06
RB5 [23]	10.8	-1.63E-03	-1.28E-03	0.11	0.10	0.06
TRIST-ER1 [21]	85	0.00E+00	-1.08E-03	1.06	0.81	0.53
Scaled Mean (85 MW)		-1.64E-03	-1.12E-03	0.89	0.72	0.44
Fractional Uncertainty				11.58%	10.36%	13.93%

3. COMPUTATIONAL NEUTRON FLUX RESULTS

Neutronics calculations are performed using the Monte Carlo N-Particle (MCNP) code, and the outputs are analyzed with Matlab. A standard HFIR MCNP model was created in 2004 by N. Xoubi and R. T. Primm III [2]. This MCNP model is based on the experimental loadings of Cycle 400 (4/27/2004–5/21/2004). The use of the Cycle 400 model as a starting point presupposes that the operating conditions in Cycle 400 are similar to those found in the experimental data. This assumption is reasonable because the core changed little between 1982 and 2004, and the experimental loading is characteristic of a normal HFIR operating cycle [2]. The MCNP model has some simplifying assumptions that may limit its accuracy, including a homogenized fuel region and target loadings.

All MCNP cases are run for 550 generations with an initial source of 100,000 neutrons. This yields fractional standard deviations of k_{eff} for all cases in the range of 0.01–0.02%. The continuous-energy library ENDF/B-VII at 293.6 K is used for cross-section data. In order to minimize perturbations of the nominal Cycle 400 composition, 11 MCNP cases are used. Each case uses the initial Cycle 400 model and modifies it for a few target locations, leaving the rest of the core as it is originally described. The target facilities in the FT and VXF positions are split into groups on the basis of radial distance from the center of the core, while the RB target facilities are split into two groups on the basis of whether they originally contained a beryllium plug. Table V shows the 11 groups created, their radial distance from the center of the core, and the target facilities that each group contains. Reactor conditions as a function of burnup are characterized by using a MCNP model of the BOC (beginning of cycle) and EOC (end of cycle).

3.1. Geometry and Materials Specifications

Initially a large number of different target geometries were investigated, and the neutron flux (particularly at fast energies) was found to be strongly dependent on the size of the water gap surrounding the target. In order to produce consistent results that show the spatial character of the neutron flux spectrum, the geometry used for each target location in a region is standardized. Each target location in the FT is modeled with JP capsule geometry because most of the

Table V. MCNP Target Group Composition

Group #	Description	Radial dist. (cm)	Radial dist. (in)	Target facilities
1	FT - Center	0	0	D4
2	FT	1.69	0.67	D3, C3, C4, D5, E5, E4
3	FT	2.93	1.15	B3, C5, E6, F5, E3, C2
4	FT	3.38	1.33	B4, D6, F6, F4, D2, B2
5	FT	4.47	1.76	A2, A3, B5, C6, E7, F7 G6, G5, F3, E2, C1, B1
6	FT - PTP	5.38	2.12	A1, A4, D7, G7, G4, D1
7	RB - 1	27.31	10.75	RB: 1B, 3A, 3B, 7A, 7B
8	RB - 2	27.31	10.75	RB: 1A, 2, 4, 5A, 5B, 6, 8
9	Inner small VXF	39.21	15.44	VXF: 1, 3, 5, 7, 9, 11, 13 15, 18, 20, 22
10	Outer small VXF	44.05	17.34	VXF: 2, 4, 8, 10, 12
11	Large VXF	46.28	18.22	VXF: 6, 14, 16, 17, 19, 21

experimental data comes from JP-type experiments. The RB and VXF facilities are modeled using dimensions from the MFE -18J capsule. Only the outer dimensions of the capsules are used; everything inside the outer diameter is homogenized.

In order to best represent the experiments, it is necessary to implement materials corresponding to those used for fluence monitors; however, the net neutron absorption added by the material chosen needs to be representative of standard HFIR target loadings. Standard loadings in an experimentally loaded target location are "equivalent to that associated with 200 g of aluminum and 35 g of stainless steel distributed uniformly over a 20-in. (50.8-cm) length."[3]

3.2. Coarse-Energy-Group Flux Spectra in FT

Calculated values for the fast ($E > 0.1$ MeV) and thermal ($E < 0.5$ eV) flux spectra at the BOC are shown in Fig. 2. The fast flux achieves a maximum value of $1.32 \cdot 10^{15} \frac{\mathrm{n}}{\mathrm{cm}^2-\mathrm{sec}}$ in the PTP facilities and decreases radially inward with location D-4 having a minimum value of $1.08 \cdot 10^{14} \frac{\mathrm{n}}{\mathrm{cm}^2-\mathrm{sec}}$. Conversely, the thermal flux increases radially inward; the two highest values of 2.21 and $2.24 \cdot 10^{15} \frac{\mathrm{n}}{\mathrm{cm}^2-\mathrm{sec}}$ are found in the HT and in the center position (D-4), respectively. Unless otherwise noted, the coarse-group flux values for target locations are about the centerline from -1.27 to 1.27 cm.

The coarse-group neutron spectra about the midplane are averaged over each MCNP group and presented in Table VI. Differences between calculated radial group flux values are significant. Thermal flux is highest at the center and decreases in the radial direction. Conversely, the fast flux is highest near the fuel in the PTP region and drops off towards the center of the FT. These

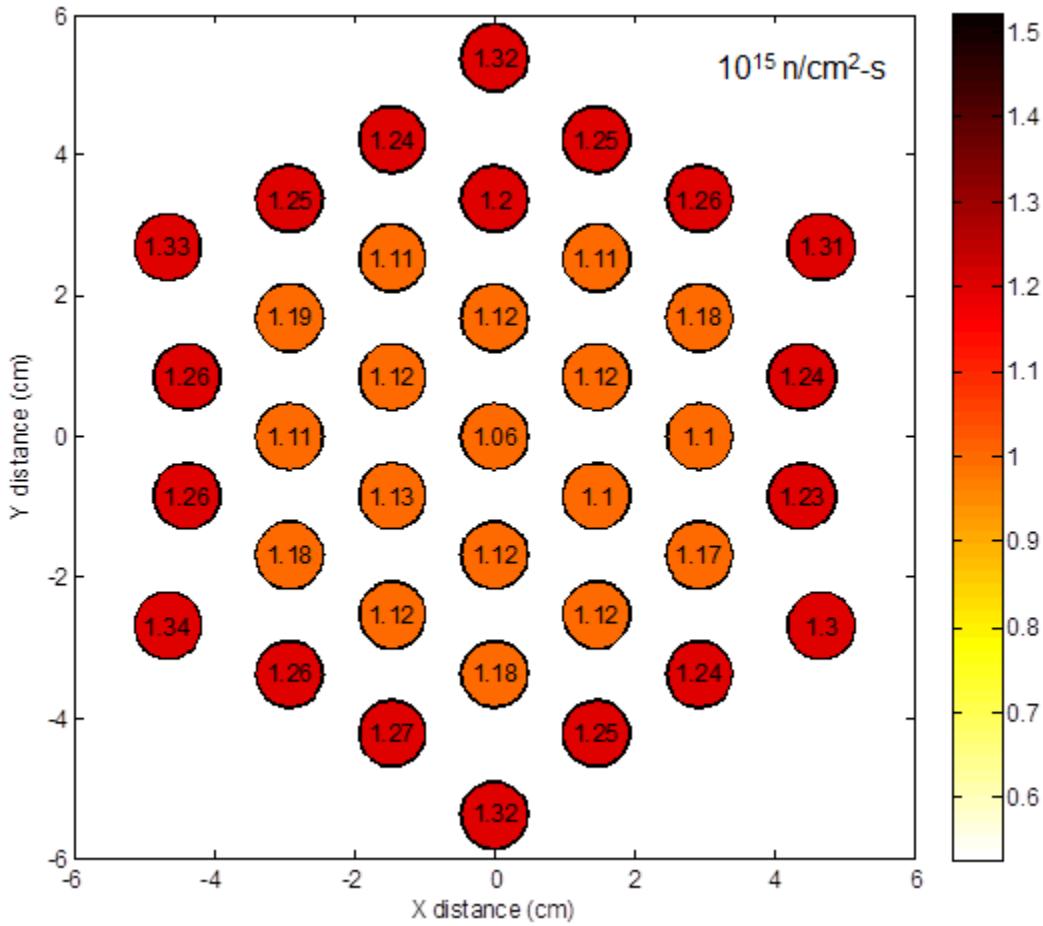

Figure 2. Fast flux in FT region at BOC.

findings conform to our expectations. However, the second and third radial groups show similar fast and thermal flux values despite their varying radial distances.

3.3. Flux Variation with Respect to Burnup

As can be seen in Table VI, differences between the BOC and EOC are small for the central FT locations but more pronounced near the outer edge. The thermal flux at BOC is shown to increase for groups five and six by 5.5 and 8.5%, respectively, and remain constant for the inner four groups. However, the fast flux uniformly decreases for all FT groups towards the EOC, having an average decrease of 14.4%. The largest variation in flux with respect to burnup is found in the RB positions. Thermal flux at the midplane increases 36%, while the axial variation flattens out. Fast flux is calculated to decrease only 3.5% from BOC to EOC.

Table VI. FT Group Flux about Midplane

Radial Group	**Neutron flux** ($10^{15}\frac{\mathrm{n}}{\mathrm{cm}^2-\mathrm{sec}}$)		
	<0.5 eV	**0.5 eV–0.1 MeV**	**>0.1 MeV**
BOC			
1 (D4)	2.29	1.31	1.08
2 (C3)	2.16	1.35	1.12
3 (B3)	2.24	1.33	1.12
4 (D6)	2.01	1.38	1.18
5 (E7)	1.81	1.42	1.25
6 (PTP-1)	1.72	1.42	1.32
BOC FT Mean	2.04	1.37	1.18
EOC			
1	2.23	1.15	0.93
2	2.06	1.18	0.96
3	2.16	1.16	0.95
4	1.98	1.21	1.01
5	1.91	1.24	1.07
6	1.88	1.25	1.12
EOC FT Mean	2.04	1.2	1.01

3.4. Axial Flux Profile in FT Region

The normalized axial flux profiles for the FT region all have the same shape and are well fit by a second-order polynomial. A typical axial thermal flux profile is shown in Fig. 3. The figure shows close correspondence between individual target locations within the PTP group, and that a second-order polynomial fits the data from PTP-2 well, yielding a R^2 value of 0.98. The normalized fast flux profile of group six (PTP locations) displays a similar shape. A least-squares regression fits the fast flux data from PTP-2 with a R^2 value of 0.99. In order to compare the MCNP axial flux distributions, all fits of axial flux profiles are done on midplane-scaled data with a second-order polynomial whose intercept is 1.

3.5. Fine-Group Analysis

Plots of flux per unit lethargy were constructed from 69-group energy tallies. Figure 4 shows a plot of flux per unit lethargy for the six radial groups in the FT. The plot shows that group one (i.e., the center of the FT) has the highest thermal peak and lowest fast peak, while group six (PTP positions) has the lowest thermal flux and highest fast flux. This is the expected result, since the PTP locations are closest to the fuel.

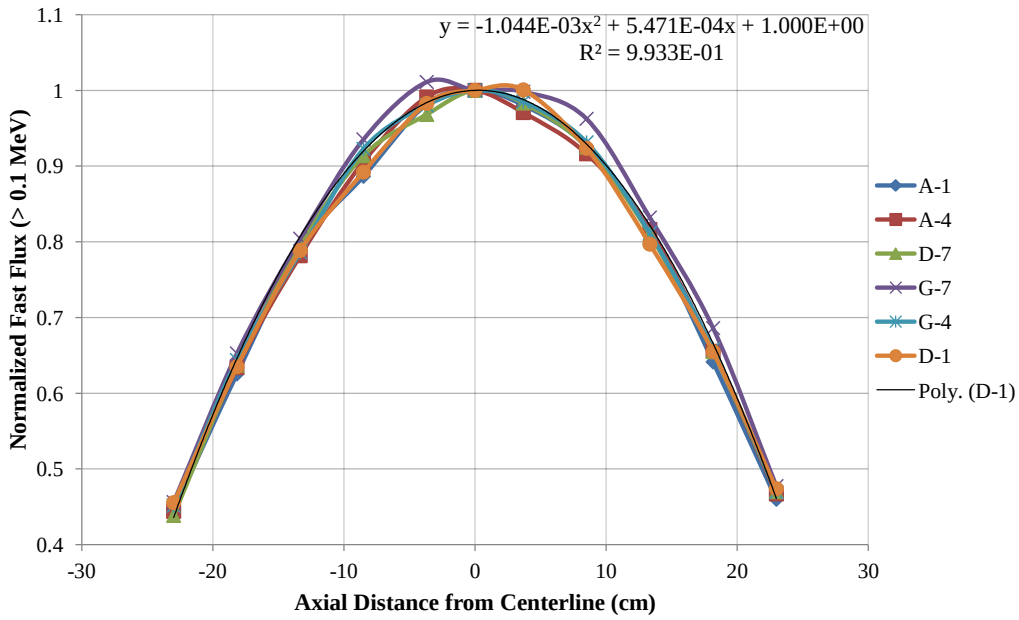

Figure 3. Fast axial flux profile in the PTP region.

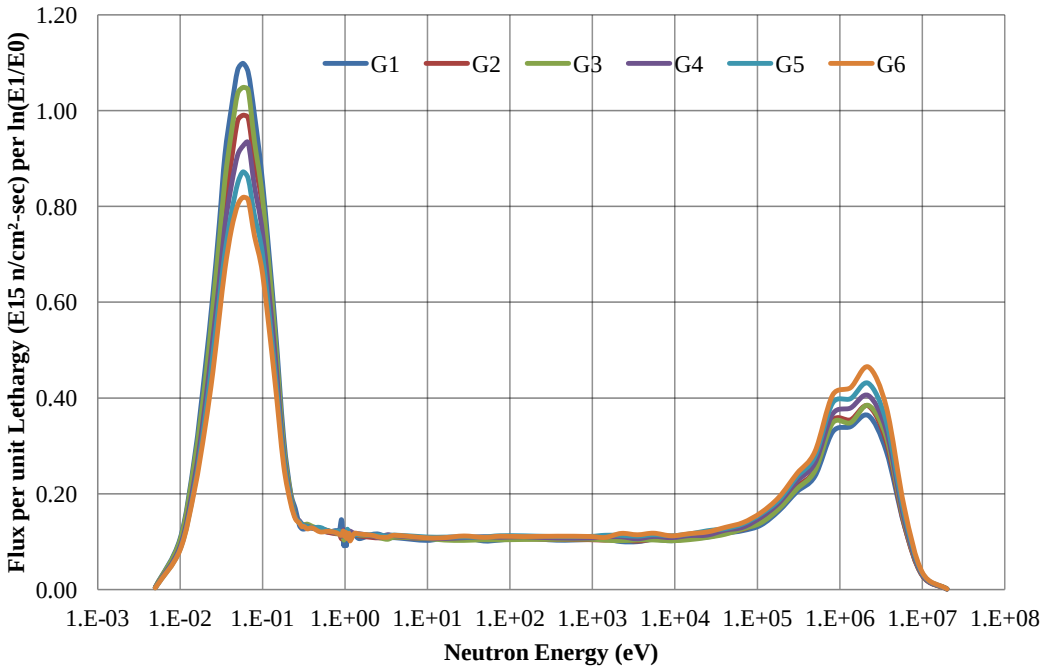

Figure 4. Flux per unit lethargy in the FT region.

4. SUMMARY OF MEASURED AND CALCULATED FLUX

A flux comparison between experiments performed in the PTP, FTT, and RB locations and the values produced by the MCNP models are shown in Table VII. Uncertainties for the experimental values are calculated as the square root of the sample variance. Experimental values for thermal flux have the largest fractional uncertainties, ranging from 4.5–14.9%, compared to uncertainties ranging from 1.5–5.9% for fast flux values. Axial fit parameters are presented according to Eq. 1. The axial flux presented in this section refers to thermal flux except for the RB shielded experiments, where it is the fit of the axial fast flux.

As is shown in Table VII, the MCNP model for the PTP locations agrees well with the average experimental thermal flux value of 1.75±0.09 $\cdot 10^{15} \frac{\mathrm{n}}{\mathrm{cm}^2-\mathrm{sec}}$, ranging from a percent difference of -1.7% at BOC to 6.9% at EOC. Fast flux in the PTP locations vary over BOC to EOC from a percent difference of 13.6% to -1.8% and have an experimental value of 1.14±0.04 $\cdot 10^{15} \frac{\mathrm{n}}{\mathrm{cm}^2-\mathrm{sec}}$. Since most experiments were performed over the duration of one or more cycles, values for neutron flux that lie between computational results for flux at BOC and EOC is expected. The axial profiles determined experimentally and computationally are similar; however, the second-order term of the fit parameter is smaller in the MCNP cases.

Table VII. Coarse Group and Axial Flux Comparison

Location	**Source**	**Fit parameter**		**Scaled flux** ($10^{15} \frac{\mathrm{n}}{\mathrm{cm}^2-\mathrm{sec}}$)		
		b	**c**	**<0.5 eV**	**Intermediate**	**>0.1 MeV**
PTP	Experimental	2.91E-04	-9.83E-04	1.75±0.09	1.38±0.05	1.14±0.04
	MCNP - BOC	5.89E-04	-9.30E-04	1.72	1.42	1.32
	MCNP - EOC	-1.56E-04	-8.99E-04	1.88	1.25	1.12
FT	Exper. (100 MW)	5.01E-04	-9.93E-04	1.82±0.24	1.35±0.03	1.12±0.02
(4.47 cm)	Exper. (85 MW)	2.14E-05	-9.93E-04	1.73±0.20	1.30±0.05	1.06±0.04
	MCNP - BOC	4.26E-04	-8.90E-04	1.81	1.42	1.25
	MCNP - EOC	-3.39E-04	-8.31E-04	1.91	1.24	1.07
RB	Exper.	-1.64E-03	-1.12E-03	0.89±0.10	0.72±0.07	0.44±0.06
	MCNP - BOC	-2.05E-03	-1.39E-03	0.79	0.73	0.46
	MCNP - EOC	-2.67E-04	-9.22E-04	1.07	0.73	0.44

All experiments which specified the position of the FT experiments (excluding PTP positions) were irradiated in the fifth radial group. Consequently, the MCNP model used to compare these results is from only the fifth group (R = 4.47 cm). Comparing the fifth MCNP group to the experimental data shows that percent change varied from 0.6% to 5.8% for thermal neutrons and from 13.2% to -1.4% for fast neutrons. The axial flux profile for thermal neutrons in this region also show MCNP results that are smaller than experimental and decrease towards the EOC.

Experimental and computational results for the RB target locations correspond closely. RB experiments report a fast flux of 0.47±0.04 and 0.46±0.04 $\cdot 10^{15} \frac{\mathrm{n}}{\mathrm{cm}^2-\mathrm{sec}}$, respectively. These experimental data points agree with the values produced by MCNP, which range from 0.46–0.44 $10^{15} \frac{\mathrm{n}}{\mathrm{cm}^2-\mathrm{sec}}$. The experimental second-order parameter of the axial fit, -1.15 $\cdot 10^{-3}$, lies between the BOC and EOC values of -1.39 $\cdot 10^{-3}$ and -0.92 $\cdot 10^{-3}$ produced by MCNP.

5. CONCLUSIONS

Experimental results for the PTP, FT, and RB target facilities were presented and compared with MCNP models of the HFIR with standard target loadings. The coarse-energy-group flux values tallied in MCNP for BOC and EOC conditions bound the reported experimental results in most cases. Reported flux values and axial distributions at a given radial distance from the center of the reactor agree well, and the flux distribution in the target facilities is largely radially symmetric. The experimental thermal flux values are found to have a significantly larger variance than values for fast flux.

ACKNOWLEDGMENTS

The authors would like to acknowledge the support of the Fusion Energy Materials Program in performing this work as well as the more than 30 years of neutron flux monitoring experiments performed in HFIR. We would also like to thank N. Xoubi and R. T. Primm III for their work in developing the HFIR 400 MCNP model.

REFERENCES

[1] "HFIR: In-Vessel Irradiation Experiment Facilities" http://neutrons.ornl.gov/facilities/HFIR/in-vessel.shtml (2011).

[2] N. Xoubi, R. T. Primm III, *Modeling of The High Flux Isotope Reactor Cycle 400*, ORNL Technical Memo, ORNL/TM-2004/251, 2004.

[3] "Experiment Facilities" http://www.ornl.gov/sci/rrd/pages/experiment.html (2011).

[4] L. R. Greenwood, "Neutron Source Characterization for Materials Experiments," *Alloy Development for Irradiation Performance* **DOE/ER-0045/11**, pp. 30-37 (1983)

[5] L. R. Greenwood, "Neutron Source Characterization for Materials Experiments," *Alloy Development for Irradiation Performance* **DOE/ER-0045/13**, pp. 13-17 (1984)

[6] L. R. Greenwood, "Fission Reactor Dosimetry - HFIR - CTR 40-45," *Damage Analysis and Fundamental Studies*, **DOE/ER-0046/19**, pp. 5-8 (1984)

[7] L. R. Greenwood, "Fission Reactor Dosimetry - HFIR - CTR 30, 36, 46," *Damage Analysis and Fundamental Studies*, **DOE/ER-0046/21**, pp. 5-9 (1985)

[8] L. R. Greenwood, "Dosimetry and Damage Analysis for HFIR-CTR-47/48," *Fusion Reactor Materials*, **DOE/ER-0313/2**, pp. 38-40 (1987)

[9] L. R. Greenwood and D. V. Steidl, "Dosimetry for The HFIR - CTR 53/54 Experiments," *Fusion Reactor Materials*, **DOE/ER-0313/8**, pp. 40-42 (1990)

[10] L. R. Greenwood and C. A. Baldwin, "Neutron Dosimetry and Damage Calculations for the HFIR-CTR-62 and 63 Irradiations," *Fusion Reactor Materials*, **DOE/ER-0313/26**, pp. 199-201 (1999)

[11] J. L. Scott, M. L. Grossbeck, and M. P. Tanaka, "Phase I HFIR Capsules - Irradiation and Postirradiation Examination," *Alloy Development for Irradiation Performance*, **DOE/ER-0045/15**, pp. 4-14, 18-21 (1985)

[12] L. R. Greenwood, "Neutron Dosimetry and Damage Calculations," *Alloy Development for Irradiation Performance*, **DOE/ER-0045/16**, pp. 17-24 (1986)

[13] L. R. Greenwood, "Measurements for the JP2, JP6, JP7 US/Japanese Experiments in HFIR," *Fusion Reactor Materials*, **DOE/ER-0313/2**, pp. 31-33 (1987)

[14] L. R. Greenwood and C. A. Seils, "Dosimetry and Damage Calculations for the JP4, JP5, and JP8 US/Japanese Experiments in HFIR," *Fusion Reactor Materials*, **DOE/ER-0313/3**, pp. 30-32 (1987)

[15] L. R. Greenwood and R. T. Ratner, "Neutron Dosimetry and Damage Calculations for the JP-10, 11, 13, and 16 Experiments in HFIR," *Fusion Materials*, **DOE/ER-0313/19**, pp. 281-285 (1995)

[16] L. R. Greenwood and R. T. Ratner, "Neutron Dosimetry and Damage Calculations for the JP-17, 18, and 19 Experiments in HFIR," *Fusion Materials*, **DOE/ER-0313/19**, pp. 286-290 (1995)

[17] L. R. Greenwood and R. T. Ratner, "Neutron Dosimetry and Damage Calculations for the HFIR-JP-23 Irradiations," *Fusion Materials*, **DOE/ER-0313/21**, pp. 229-232 (1996)

[18] L. R. Greenwood and C. A. Baldwin, "Neutron Dosimetry and Damage Calculations for the HFIR-JP-9, -12, and -15 Irradiations," *Fusion Materials*, **DOE/ER-0313/23**, pp. 301-304 (1997)

[19] L. R. Greenwood and C. A. Baldwin, "Neutron Dosimetry and Damage Calculations for the HFIR-JP-20 Irradiation," *Fusion Materials*, **DOE/ER-0313/23**, pp. 305-308 (1997)

[20] S. T. Mahmood, et al., "Neutron Dosimetry of the HFIR Hydraulic Facility," *ORNL Technical Memo*, **ORNL/TM-12831** (1995)

[21] L. R. Greenwood and C. A. Baldwin, "Neutron Dosimetry and Damage Calculations for the TRIST ER-1 Experiment in HFIR," *Fusion Reactor Materials*, **DOE/ER-0313/26**, pp. 194-198 (1999)

[22] L. R. Greenwood, "Reanalysis of the HFIR-RB1, RB2 Experiments," *Alloy Development for Irradiation Performance*, **DOE/ER-0045/15**, pp. 12-14 (1985)

[23] L. R. Greenwood, "Hafnium Shielding Tests in HFIR-RB Positions and Reanalysis of the HFIR-RB1, -RB2 Experiment," *Damage Analysis and Fundamental Studies*, **DOE/ER-0046/23**, pp. 9-15 (1985)